PCCP

ROYAL SOCIETY OF CHEMISTRY

PAPER

Cite this: *Phys. Chem. Chem. Phys.*, 2020, **22**, 24109

Prediction of two-dimensional ferromagnetic ferroelectric VOF_2 monolayer

Hai-Peng You, Ning Ding, Jun Chen and Shuai Dong *

Received 9th August 2020,
Accepted 28th September 2020

DOI: 10.1039/d0cp04208k

rsc.li/pccp

Nowadays, designing and searching for materials with multiple functional characteristics are the keys to achieving high-performance electronic devices. Among many candidates, two-dimensional multiferroic materials have great potential to be applied in highly integrated magnetoelectric devices, such as high-density non-volatile memories. Here, we predict a two-dimensional material, VOF_2 monolayer, to possess intrinsic ferroelectric and ferromagnetic properties. The VOF_2 monolayer owns the largest in-plane ferroelectric polarization (332 pC m^{-1}) in the family of VOX_2 (X: halogen) oxyhalides. Different from other VOX_2 monolayers whose magnetic ground states are antiferromagnetic or noncollinear spiral textures, the VOF_2 monolayer owns a robust ferromagnetic ground state, which is rare but highly desirable. Our theoretical prediction provides a good candidate and starting point for the further pursuit of more two-dimensional multiferroic materials with high-performance magnetoelectricity.

Introduction

In the last decade, research on two-dimensional (2D) van der Waals (vdW) materials have increased rapidly due to their broad application prospects in the field of microelectronics and optoelectronics. 2D materials with intrinsic ferro-type properties, like ferroelectricity and ferromagnetism, emerged as attractive new branches of 2D families, such as $CuInP_2S_6$,[1–4] In_2Se_3,[5,6] SnTe,[7] $Cr_2Ge_2Te_6$,[8] and CrI_3.[9,10] Among three-dimensional (3D) crystals,[11] the ferro-materials are high-value functional materials,[12–14] and have been broadly used in many devices. The 2D forms of these ferro-ordered materials can be even more interesting and useful, considering the urgent demand for miniaturization of devices.

Encouraged by the recent success in 2D ferroelectric (FE) materials and ferromagnetic (FM) materials,[15–19] investigations on 2D multiferroics are also in progress.[20,21] Multiferroics, coupling ferroelectricity and magnetism in single-phase materials, can be much helpful to realize ultra-high-speed reading and writing for data storages.[22–26] In the past decade, significant progresses have been made in the field of multiferroicity, and thus the physical understanding of multiferroic materials has been much deepen. Even through, almost all known multiferroics are antiferromagnetic (AFM) in the three-dimensional (3D) crystals, while the desired materials with intrinsic ferromagnetism and ferroelectricity remain rare. Fortunately, Tan *et al.* recently predicted a series of 2D multiferroic oxyhalides VOX_2 (X = Cl, Br, and I), among which the magnetic ground state of VOI_2 was predicted to be FM.[27] In contrast, $VOCl_2$ and $VOBr_2$ were proposed to be AFM, as confirmed by Ai *et al.*[28]

However, our following study found that VOI_2 could not possess ferromagnetism and ferroelectricity simultaneously.[29] The crucial reason is that the strong spin–orbit coupling (SOC) of heavy element iodine can lead to a large Dzyaloshinskii–Moriya interaction for the polar structure, which distorts the FM texture to a short-periodic spiral one. Thus, heavy elements should be avoided if one wishes to stabilize ferromagnetism in ferroelectric systems. With this idea, we will study the end member in the opposite side, *i.e.* VOF_2, which was missed in previous studies,[27,28] to pursue the possible coexistence of ferromagnetism and ferroelectricity.

Computational methods

The density functional theory (DFT) calculations were performed using the Vienna *ab initio* Simulation Package (VASP).[30,31] The projector-augmented wave (PAW) potentials with generalized gradient approximation of Perdew–Burke–Ernzerhof (GGA-PBE)[32] formulation were used with a cut-off energy of 550 eV. In order to search for a possible magnetic ground state of VOF_2, a $2 \times 2 \times 1$ supercell was constructed. A $9 \times 9 \times 1$ k-grid was adopted to sample the Brillouin zone utilizing the Monkhorst–Pack k-points scheme for the unit cell. [33] The energy convergence criterion was 10^{-6} eV and the criterion of Hellmann–Feynman force was 0.005 eV $Å^{-1}$ throughout the structural relaxation. The FE polarization was obtained by the standard Berry phase method.[34] A vacuum layer of 16 Å was added in the out-of-plane direction to avoid interactions between adjacent layers. The vdW

School of Physics, Southeast University, Nanjing 211189, China.
E-mail: sdong@seu.edu.cn

interaction was described by the DFT-D2 functional.[35] The DFPT + Phonopy method was employed to calculate phonon spectra.[36] The GGA+U approach was adopted for the 3d orbitals of the transition metal V.[37] For comparison, the hybrid functional calculations based on the Heyd–Scuseria–Ernzerhof (HSE06) exchange were also carried out.[38] According to literature, the coefficient AEXX = 0.1 for V ion is a proper choice.[39] To analyze the thermodynamic properties, the Markov-chain Monte Carlo (MC) method with Metropolis algorithm was employed to simulate the magnetic phase transition under finite temperature. The MC simulation was conducted on a 36 × 36 lattice with periodic boundary conditions, and larger lattices were also tested to confirm the physical results. The initial 2×10^4 MC steps were discarded for thermal equilibrium, and the following 2×10^4 MC steps were retained for statistical averaging of the simulation. To avoid the possible trapping in local minimal energy, the quenching process was used for temperature scanning. To characterize the magnetic phase transitions, the specific heat was calculated to determine the critical temperature.

Results and discussions

Structure and stability

Since the experimental data are available only for oxyhalide $VOCl_2$ bulk,[40] the initial structure of the VOF_2 monolayer can be obtained by replacing Cl with F. Considering the fact that element F is more electronegative than Cl, VOF_2 should be more chemically stable than $VOCl_2$ against oxygen and moisture.

Then the structural relaxation was performed. As shown in Fig. 1(a), the crystal structure of the VOF_2 monolayer is orthorhombic (space group No. 25 *Pmm*2) after optimization. The V ion, caged in the O_2F_4 octahedron, shifts towards one oxygen ion, which breaks the spatial inversion symmetry along the *a*-axis and leads to a polar structure. The optimized lattice structural parameters of the VOF_2 monolayer by PBE and HSE06 can be found in Table 1. Comparing with other oxyhalides VOX_2 (X = Cl, Br, and I),[27] VOF_2 has a smaller *b* due to the smaller radius of F^{1-} than other halogen ions.

Due to the anisotropic octahedral crystal field, the 3d orbitals of V ion are split into four energy levels: d_{z^2}, $d_{x^2-y^2}$, d_{xz}/d_{yz}, and d_{xy} orbitals, respectively. The d_{xy} orbital has the lowest energy, and thus, the single unpaired electron of V^{4+} should occupy this d_{xy} orbital, as shown in Fig. 1(c). For most proper ferroelectrics, the empty d orbitals are preferred, *i.e.* the empirical d^0 rule. Here, although the electronic structure is not d^0 but d^1, the orbitals d_{z^2} and d_{xz}/d_{yz} with lobes pointing along the *z*-direction (*i.e.* the *a*-axis) are empty, which can mimic the d^0 effect for FE polarization along the *a*-axis. The orbital-projected electron density of state (PDOS) of the VOF_2 monolayer is displayed in Fig. 2(a). Indeed, the topmost valence band near the Fermi energy level is from orbital d_{xy}, in consistency with the occupied charge density presented in Fig. 1(c). Also, the VOF_2 monolayer is a semiconductor, with a band gap of 0.6 eV in pure GGA-PBE calculation, which is usually underestimated.

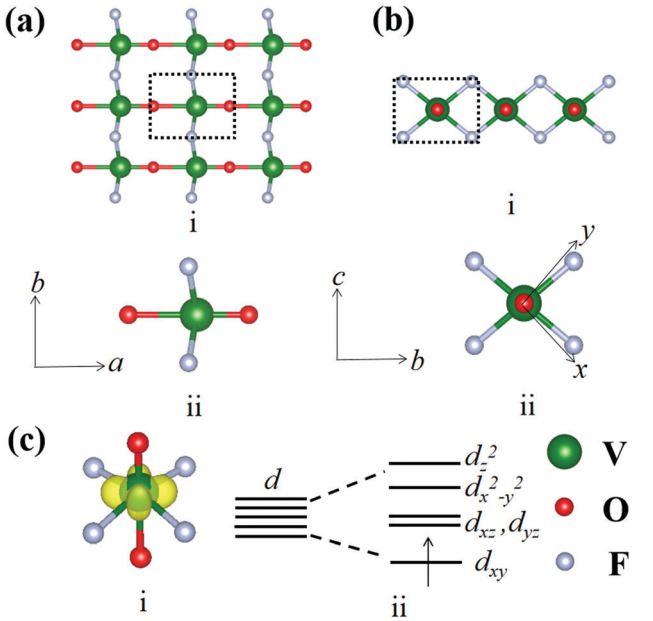

Fig. 1 Schematic of VOF_2 structure, which is similar to other VOX_2. (a) Top view of the VOF_2 monolayer. i: a 3 × 3 supercell; ii: a minimal unit-cell. (b) Side-view along the *a*-direction. i: a 3 × 1 supercell; ii: a minimal unit-cell. The dashed rectangles in (a) i and (b) i indicate the primitive cells. The *x*–*y* axis of the octahedron is also indicated in (b) ii. (c) The orbital structure. Left: The charge density of the occupied d-orbital. Right: The orbital splitting due to the crystal field.

Table 1 DFT optimized structural parameters of the VOF_2 monolayer by PBE and HSE06 methods, which are quite close to each other

	Lattice constants	Bond lengths	Bond angels
PBE	a = 3.783 Å	1.973 Å (V–F)	180° (O–V–O)
	b = 3.033 Å	2.152 Å (V–O_1)	82.5° (F–V–O_1)
		1.630 Å (V–O_2)	97.5° (F–V–O_2)
HSE06	a = 3.738 Å	1.954 Å (V–F)	180° (O–V–O)
	b = 3.013 Å	2.133 Å (V–O_1)	82.7° (F–V–O_1)
		1.604 Å (V–O_2)	97.3° (F–V–O_2)

Furthermore, the phonon spectrum of the VOF_2 monolayer was obtained to verify the dynamic stability. As shown in Fig. 2(b), no obvious imaginary frequency mode is evidenced for the optimized FE state, implying that its FE monolayer is dynamically stable. The cleavage energy (E_{cl}) was also calculated.[41] By increasing the separation distance d and keeping a 20 Å vacuum layer, the exfoliation process was simulated, as shown in Fig. 2(c). Compared with the E_{cl} of graphite (0.37 J m^{-2}), VOF_2 owns a smaller value (0.17 J m^{-2}) due to its weaker interlayer vdW interaction, close to that of the $VOCl_2$ monolayer (0.16 J m^{-2}).[28]

Ferroelectricity & magnetism

Subsequently, we studied the ferroelectricity and magnetism of the VOF_2 monolayer. Obviously, the displacement of the V ion from the center of an octahedron breaks the inversion symmetry and thus generates a spontaneous polarization. In our DFT calculation, the FE polarization of the VOF_2 monolayer is estimated as 332 pC m^{-1}, larger than that of other VOX_2,

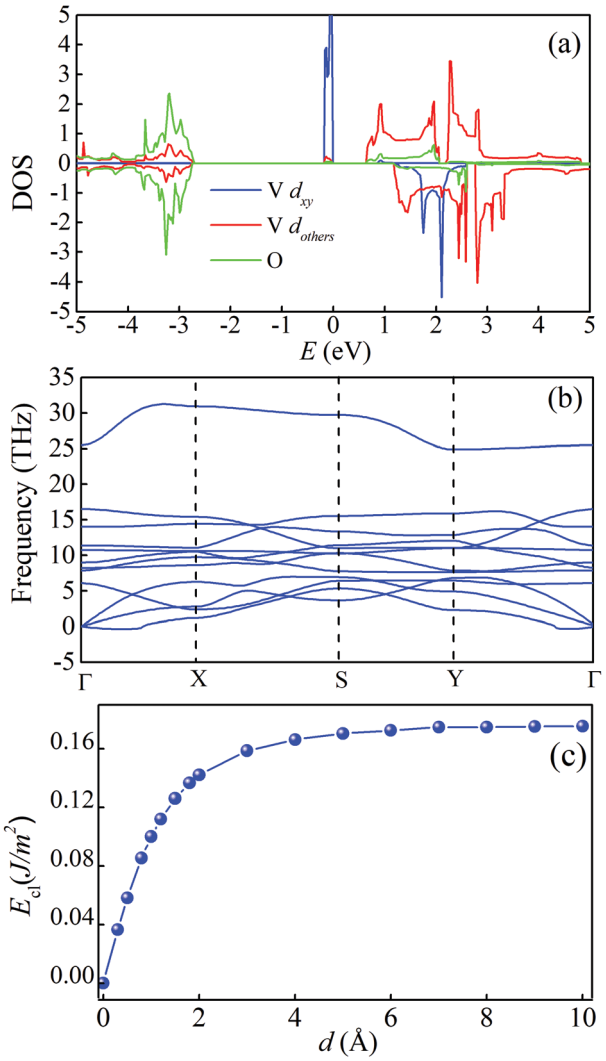

Fig. 2 (a) The PDOS of the VOF_2 monolayer. It is clear that the topmost valence band is from V's d_{xy} orbital, while all other V's orbitals form the conducting bands. (b) The phonon spectra of the VOF_2 monolayer. (c) The cleavage energy E_{cl} as a function of separation distance d in the process of exfoliating the VOF_2 monolayer from its bulk.

as seen in Fig. 3(a). The polarization reversal process can also be simulated by choosing an appropriate switching path, *i.e.* by shifting the position of V, as illustrated in Fig. 3(b). If the lattice constants a and b of the FE phase are fixed during this process, the energy barrier for FE switching is 0.33 eV. However, if the lattice constants a and b can adapt coordinately during the switching, the actual energy barrier for the VOF_2 monolayer reduces to 0.15 eV, smaller than that of $VOCl_2$.[28] This barrier can be considered as an upper limit for real materials.

The magnetism comes from the spin of an unpaired electron in the d_{xy} orbital of V^{4+} ion, and thus, the local magnetic moment is about 1 μ_B/V. In order to study the magnetic ground state of VOF_2, a 2 × 2 × 1 supercell is adopted, in which four collinear magnetic orders can be defined: FM, AFM(I), AFM(II), and AFM(III), as shown in Fig. 3(d). The energy differences of these magnetic orders obtained in our DFT calculation are shown in Table 2, indicating that the FM order is more stable than other AFM orders.

Then the magnetic exchanges, including the nearest-neighbor J_a and J_b along the a- and b-direction, respectively, and the next-nearest-neighbor J_{ab}, are extracted using the following equations:

$$\begin{aligned} E_{\mathrm{FM}} &= E_0 + 4J_a + 4J_b + 8J_{ab}, \\ E_{\mathrm{AFM(I)}} &= E_0 - 4J_a + 4J_b - 8J_{ab}, \\ E_{\mathrm{AFM(II)}} &= E_0 + 4J_a - 4J_b - 8J_{ab}, \\ E_{\mathrm{AFM(III)}} &= E_0 - 4J_a - 4J_b + 8J_{ab}, \end{aligned} \quad (1)$$

where E_0 denotes the energy of the nonmagnetic part, and all energies are recalculated based on the optimized lattice with FM state. The calculated values of the exchanges are shown in Table 3. All three exchanges tend to form FM coupling, and the exchange J_b plays a leading role, which is reasonable considering the d_{xy} orbital shape.

Besides the exchanges, magnetic anisotropy is essential to stabilize a long-range magnetic order in the 2D limit according to the Mermin–Wagner theory.[42] By considering the SOC coupling, magnetic anisotropy is obtained by calculating the energy of the FM orders with spin pointing along the [100], [010], and [001] directions. The calculated magnetic anisotropy energy values are 0.02 meV (K_b) and 0.05 meV (K_c), as shown in Table 3, implying a magnetic easy axis along the a-axis.

Besides, the anti-symmetric Dzyaloshinskii–Moriya interaction may also affect the magnetic ground state.[43,44] For example, for VOI_2, although an FM ground state was predicted,[26] our current work suggests that the strong Dzyaloshinskii–Moriya interaction distorts the spin texture to a spiral one, instead of a collinear FM one. This Dzyaloshinskii–Moriya interaction directly associates with the FE distortion. To calculate the Dzyaloshinskii–Moriya coefficients, the 3 × 1 × 1 and 1 × 3 × 1 supercells are constructed and the non-collinear spin angles between neighboring V ions are set as 120°, as shown in Fig. 3(e). The 120° non-collinear configurations can converge well in our calculation, and the output magnetic textures are corrected as expected. Considering the crystal symmetry, only the a-component of D_a and c-component of D_b are allowed to be nonzero. The a-component of D_a remains too small in the DFT calculation, and the c-component of D_b is estimated as 0.09 meV, as summarized in Table 3. The weak magnetocrystalline anisotropy and the Dzyaloshinskii–Moriya interaction are reasonably small because here only light elements, namely vanadium, oxygen, and fluorine, are present. Thus, it is safe to conclude that VOF_2's ground state is FM.

In principle, the DFT calculation works at zero-temperature without thermal effect, while the MC simulation can deal with the temperature-dependent phase transition. Therefore, using the above-mentioned exchange interactions, magnetic anisotropic coefficient, and the Dzyaloshinskii–Moriya interaction, an MC simulation on the Heisenberg spin model was performed to trace the temperature dependence of magnetism. The spin

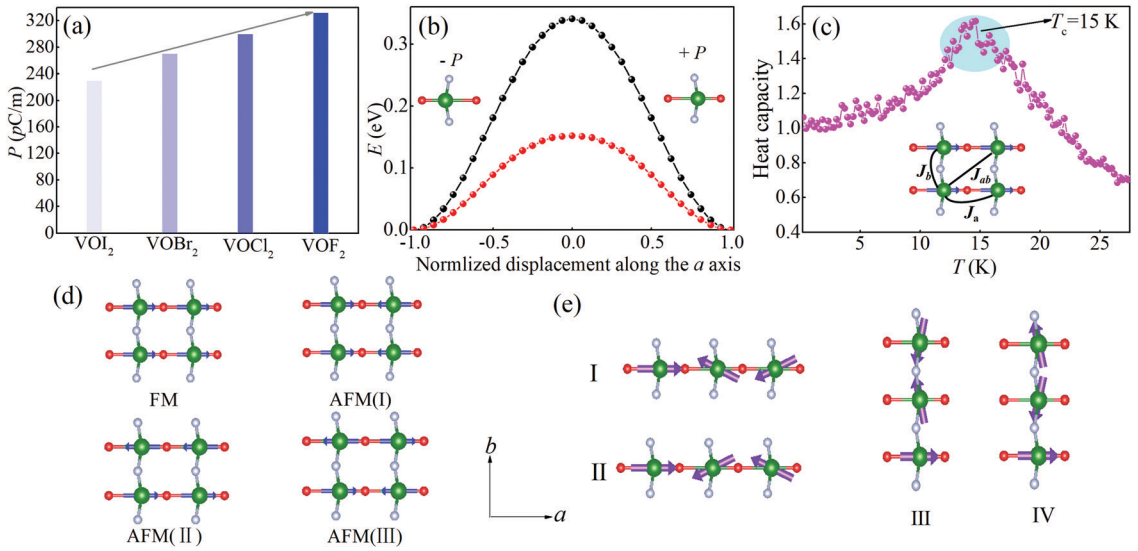

Fig. 3 (a) Comparison of calculated polarization of VOX_2 (X = I, Br, Cl, and F). (b) Energy barrier for FE switching, as a function of FE displacement of V ion. Black and red curves: the lattice constants (*a* and *b*) are unchanged and changed during the switching, respectively. Insets: $+P$ and $-P$ denote the polarization directions (c) the MC simulated heat capacity as a function of temperature (T) for the VOF_2 monolayer. Inset: The exchange paths between V ions. (d and e) Schematic of magnetic orders considered in our DFT calculation. (d) Four types of collinear magnetic orders: FM, AFM(I), AFM(II), and AFM(III). (e) Four types of 120° non-collinear magnetic orders.

Table 2 DFT energy difference of four types of magnetic orders and the energy of FM order (in meV)

ΔE_{FM}	$\Delta E_{AFM(I)}$	$\Delta E_{AFM(II)}$	$\Delta E_{AFM(III)}$
0	6	36	31

Table 3 Nearest-neighbor exchanges along the *a* and *b*-directions (J_a and J_b), next-nearest-neighbor exchange (J_{ab}), magnetic anisotropic coefficient, Dzyaloshinskii–Moriya vectors, extracted from DFT energies. The spin is normalized to unit one. Those components below 0.01 meV are set as zero for D_a and D_b

J_a	J_b	J_{ab}	K_b	K_c	D_a	D_b
−0.06	−3.81	−0.34	0.02	0.05	(0, 0, 0)	(0, 0, 0.09)

model Hamiltonian is written as follows:

$$H = J_a \sum_{\langle i,j\rangle_a} S_i \cdot S_j + J_b \sum_{\langle m,n\rangle_b} S_m \cdot S_n + J_{ab} \sum_{\langle\langle q,w\rangle\rangle} S_q \cdot S_w + \sum_i \left[K_b (S_i^y)^2 + K_c (S_i^z)^2\right] + D_a \cdot \sum_{\langle i,j\rangle_a} S_i \times S_j + D_b \cdot \sum_{\langle m,n\rangle_b} S_m \times S_n, \quad (2)$$

where S_i is the normalized vector of spin (*i.e.* $|S| = 1$) at site *i*; $\langle\ \rangle_{a/b}$ represents the nearest neighbor along the *a*-/*b*-direction; and $\langle\langle\ \rangle\rangle$ represents the next nearest neighbor along the diagonal direction. K_b and K_c are the magnetic anisotropy coefficients in/out of the plane. D_a and D_b represent anti-symmetric Dzyaloshinskii–Moriya interactions along *a*-/*b*-direction. According to the specific heat curve shown in Fig. 3(c), a peak occurs around 15 K, suggesting a magnetic phase transition. The MC snapshot (not shown here) also confirms the FM texture. Last, we have to admit that the parameters used in the MC simulation are based on the zero-temperature DFT calculation, which is qualitatively reasonable.

The effect of additional *U*

Based on pure spin-polarized GGA calculation, above results have revealed that the VOF_2 monolayer is a rare intrinsic 2D FE and FM material. However, it is essential to double-check the influence of Hubbard U correction, considering the valence electron is from a 3d orbital. Then, the GGA+U method was adopted to re-check the structure and ferroelectric and magnetic properties of the VOF_2 monolayer.

As shown in Fig. 4(a), the lattice constants *a* and *b* do change obviously with an increasing U_{eff} value, *e.g.* within ±2.5%. In addition, the band gap increases from the original value of 0.6 eV to 2.1 eV (when U_{eff} = 3 eV). Meanwhile, the FE polarization reduces from 332 pC m^{-1} to 264 pC m^{-1}, as shown in Fig. 4(b). The physical reason is that the increased U_{eff} suppresses the d–p orbital hybridization between V and O, *i.e.* the driving force of its proper ferroelectricity. The energy barrier for FE switching also decreases with increasing U_{eff}, *e.g.* 0.095 eV when U_{eff} = 2 eV. We also re-calculated the energies of four magnetic orders. Despite the value of U_{eff}, the energies of AFM configurations are always higher than the FM one, as shown in Fig. 4(c).

Thus, it is safe to conclude that the magnetic ground state of the VOF_2 monolayer is FM and FE, which will not be altered by the choice of Hubbard U in DFT calculation.

Strain effect

In comparison with 3D crystals, one advantage of 2D materials is their structural flexibility. The magnetic and electronic structures

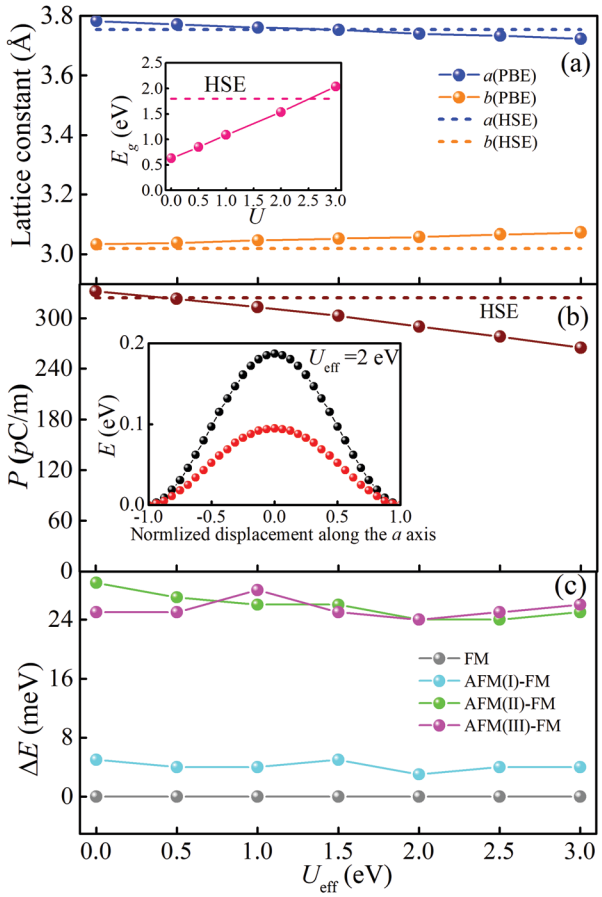

Fig. 4 (a) Lattice constants *a* and *b*, (b) FE polarization, and (c) energy differences of magnetic states as a function of U_{eff}. The HSE06 results are also presented as broken lines for comparison. Inset of (a): Band gap. Inset of (b): Energy barrier for FE switching when U_{eff} is 2 eV. Black and red curves correspond to the cases of lattice constants unchanged and changed during the process.

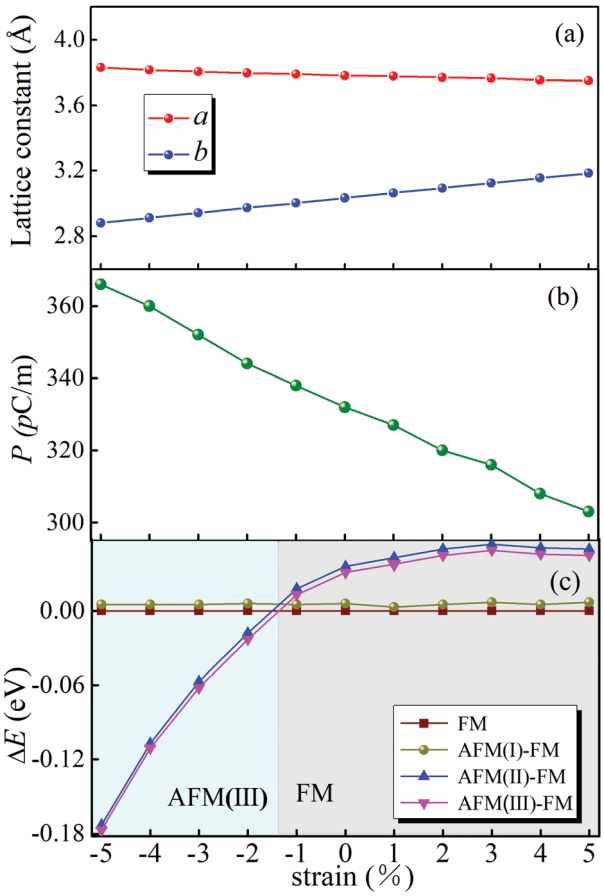

Fig. 5 (a) Lattice constants *a* and *b*, (b) ferroelectric polarization, and (c) energy differences of magnetic states as a function of uniaxial strain applied along the *b*-direction. The magnetic ground state changes from the FM one in the unstrained condition to the AFM(III) one under a moderate compressive strain.

may be tunable by stress.[45] To investigate this effect, we applied the uniaxial compressive/tensile strain from −5% to +5% along the *b*-axis, and then the lattice constant along the *a*-axis and ions' positions were optimized accordingly. As shown in Fig. 5(a), the lattice constant *a* changes almost linearly as a function of strain, in contrast to the tendency of *b*-axis but with a relatively smaller magnitude, *i.e.* from +1.3% to −0.8%. In other words, the stiffness along the *b*-axis is softer and that along the *a*-axis is harder.

Fig. 5(b) depicts the strain dependent FE polarization, which decreases with the decreasing lattice constant *a*, as expected. Or in other words, the compressive strain along the *b*-axis can enhance the FE polarization.

Most interestingly, there is competition between the FM order and the AFM(III) order. The AFM(III) state owns a lower energy than the FM one when the compressive strain goes beyond −1%, implying a magnetic phase transition for the VOF_2 monolayer.

In short, the compressive strain along the *b*-axis (or tensile strain along the *a*-axis) is an effective method to tune the multiferroicity of the VOF_2 monolayer: not only to enhance its FE polarization but also to change the magnetic ground state.

Conclusion

In summary, we have performed a systematic DFT calculation on a 2D oxyhalide VOF_2 monolayer, covering its crystal structure, electronic properties, structural stability, FE polarization, as well as its magnetism. Our results suggest that VOF_2 is an intrinsic 2D multiferroic material with rare coexistence of ferromagnetism and ferroelectricity. Furthermore, the uniaxial strain can effectively tune its FE polarization and magnetic ground state. Our theoretical work predicts a potential 2D multiferroic material with highly desired properties, which needs further experimental verification.

Conflicts of interest

The authors declare no competing financial interest.

Acknowledgements

This work was supported by the National Natural Science Foundation of China (Grants No. 11834002 and 11674055).

Computing resources used in this work were mainly provided by the Big Data Center of Southeast University.

References

1 F. C. Liu, L. You, K. L. Seyler, X. B. Li, P. Yu, J. H. Lin, X. W. Wang, J. D. Zhou, H. Wang, H. Y. He, S. T. Pantelides, W. Zhou, P. Sharma, X. D. Xu, P. Ajayan, J. L. Wang and Z. Liu, Room-temperature ferroelectricity in $CuInP_2S_6$ ultrathin flakes, *Nat. Commun.*, 2016, **7**, 12357.

2 L. You, Y. Zhang, S. Zhou, A. Chaturvedi, S. A. Morris, F. C. Liu, L. Chang, D. Lchinose, H. Funakubo, W. J. Hu, T. Wu, Z. Liu, S. Dong and J. L. Wang, Origin of giant negative piezoelectricity in a layered van der Waals ferroelectric, *Sci. Adv.*, 2019, **5**, 4.

3 S. Zhou, L. You, A. Chaturvedi, S. A. Morris, J. S. Herrin, N. Zhang, A. Abdelsamie, Y. Z. Hu, J. Q. Chen, Y. Zhou, S. Dong and J. L. Wang, Anomalous polarization switching and permanent retention in a ferroelectric ionic conductor, *Mater. Horiz.*, 2020, **7**, 263–274.

4 S. Zhou, L. You, H. L. Zhou, Y. Pu, Z. G. Gu and J. L. Wang, van der Waals layered ferroelectric $CuInP_2S_6$: Physical properties and device applications, *Front. Phys.*, 2021, **16**, 13301.

5 C. X. Zheng, L. Yu, L. Zhu, J. Collins, D. Kim, Y. D. Lou, C. Xu, M. Li, Z. Wei, Y. P. Zhang, M. T. Edmonds, S. Q. Edmonds, J. Seidel, Y. Zhu, J. Z. Liu, W. X. Tang and M. S. Fuhrer, Room temperature in-plane ferroelectricity in van der Waals In_2Se_3, *Sci. Adv.*, 2018, **4**, 7.

6 W. J. Ding, J. B. Zhu, Z. Wang, Y. F. Gao, D. Xiao, Y. Gu, Z. Y. Zhang and W. G. Zhu, Prediction of intrinsic two-dimensional ferroelectrics in In_2Se_3 and other III_2–VI_3 van der Waals materials, *Nat. Commun.*, 2017, **8**, 14956.

7 K. Chang, J. W. Liu, H. C. Lin, N. Wang, K. Zhao, A. M. Zhang, F. Jin, Y. Zhong, X. P. Hu, W. H. Duan, Q. M. Zhang, L. Fu, Q. K. Xue, X. Chen and S. H. Ji, Discovery of robust in-plane ferroelectricity in atomic-thick SnTe, *Science*, 2016, **353**, 274–278.

8 C. Gong, L. Li, Z. L. Li, H. W. Ji, A. Stern, Y. Xia, T. Cao, W. Bao, C. Z. Wang, Y. Wang, Z. Q. Qiu, R. J. Cava, S. G. Louie, J. Xia and X. Zhang, Discovery of intrinsic ferromagnetism in two-dimensional van der Waals crystals, *Nature*, 2017, **546**, 265–269.

9 B. Huang, G. Clark, E. Navarro-Moratalla, D. R. Klein, R. Cheng, K. L. Seyler, D. Zhong, E. Schmidgall, M. A. McGuire, D. H. Cobden, W. Yao, D. Xiao, P. Jarillo-Herrero and X. D. Xu, Layer-dependent ferromagnetism in a van der Waals crystal down to the monolayer limit, *Nature*, 2017, **546**, 270–273.

10 Y. H. Zhao, L. F. Ling, Q. H. Zhou, Y. H. Li, S. J. Yuan, Q. Chen, S. Dong and J. L. Wang, Surface vacancy-induced switchable electric polarization and enhance ferromagnetism in monolayer metal trihalides, *Nano Lett.*, 2018, **18**, 2943–2949.

11 Y. Ji, K. W. Zhang and Y. Yang, A one-structure-based multieffects coupled nanogenerator for simultaneously scavenging thermal, solar, and mechanical energies, *Adv. Sci.*, 2018, **5**, 1700622.

12 N. Ma and Y. Yang, Enhanced self-powered UV photoresponse of ferroelectric $BaTiO_3$ materials by pyroelectric effect, *Nano Energy*, 2017, **40**, 352–359.

13 N. Ma and Y. Yang, Boosted photocurrent in ferroelectric $BaTiO_3$ materials via two dimensional planar-structured contact configurations, *Nano Energy*, 2018, **50**, 417–424.

14 N. Ma, K. W. Zhang and Y. Yang, Photovoltaic-pyroelectric coupled effect induced electricity for self-powered photodetector system, *Adv. Mater.*, 2017, **29**, 1703694.

15 Q. Gao, H. L. Wang, L. F. Zhang, S. L. Hu and Z. P. Hu, Computational study on the half-metallicity in transition metal-oxide-incoprated 2D g-C_3N_4 nanosheets, *Front. Phys.*, 2018, **13**, 138108.

16 J. H. Feng, G. Li, X. F. Meng, X. D. Jian, Z. H. Dai, Y. C. Zhao and Z. Zhou, Computationally predicting spin semiconductors and half metals from doped phosphorene monolayers, *Front. Phys.*, 2019, **14**, 43604.

17 Y. Xie, J. S. Feng, H. J. Xiang and X. G. Gong, Interplay of strain and magnetism in FeSe monolayers, *Chin. Phys. Lett.*, 2019, **36**, 056801.

18 Y. Gong, J. W. Guo, J. H. Li, K. J. Zhu, M. H. Liao, X. Z. Liu, Q. H. Zhang, L. Gu, L. Tang, X. Feng and D. Zhang, *et al.*, Experimental realization of an intrinsic magnetic topological insulator, *Chin. Phys. Lett.*, 2019, **36**, 076801.

19 M. H. Wu and P. Jena, The rise of two-dimensional van der Waals ferroelectrics, *Wiley Interdiscip. Rev.: Comput. Mol. Sci.*, 2018, **8**, e1365.

20 T. Hu and E. J. Kan, Progress and prospects in low-dimensional multiferroic materials, *Wiley Interdiscip. Rev.: Comput. Mol. Sci.*, 2019, **9**, e1409.

21 X. Tang and L. Z. Kou, Two-dimensional ferroics and multiferroics: platforms for new physics and applications, *J. Phys. Chem. Lett.*, 2019, **10**, 6634–6649.

22 S. Dong, H. J. Xiang and E. Dagotto, Magnetoelectricity in multiferroics: a theoretical perspective, *Natl. Sci. Rev.*, 2019, **6**, 629–641.

23 S. Dong, J. M. Liu, S.-W. Cheong and Z. F. Ren, Multiferroic materials and magnetoelectric physics: symmetry, entanglement, excitation, and topology, *Adv. Phys.*, 2015, **64**, 519–626.

24 X. Huang and S. Dong, Ferroelectric control of magnetism and transport in oxide heterostructures, *Mod. Phys. Lett. B*, 2014, **28**, 1430010.

25 S.-W. Cheong and M. Mostovoy, Multiferroics: a magnetic twist for ferroelectricity, *Nat. Mater.*, 2007, **6**, 13–20.

26 R. Ramesh and N. A. Spaldin, Multiferroics: Progress and prospects in thin films, *Nat. Mater.*, 2007, **6**, 21–29.

27 H. X. Tan, M. L. Li, H. T. Liu, Z. R. Liu, Y. C. Li and W. H. Duan, Two-dimensional ferromagnetic-ferroelectric multiferroics in violation of the d^0 rule, *Phys. Rev. B.*, 2019, **99**, 195434.

28 H. Q. Ai, X. H. Song, S. Y. Qi, W. F. Li and M. W. Zhao, Intrinsic multiferroicity in two-dimensional $VOCl_2$ monolayer, *Nanoscale*, 2019, **11**, 1103.

29 N. Ding, J. Chen, S. Dong and A. Stroppa, Ferroelectricity and ferromagnetism in VOI_2 monolayer: the role of Dzyaloshinskii-Moriya interaction, *Phys. Rev. B*, 2020, **102**, 165129.
30 G. Kresse and J. Furthmüller, Efficient iterative schemes for ab initio total-energy calculations using a plane-wave basis set, *Phys. Rev. B: Condens. Matter Mater. Phys.*, 1996, **54**, 11169–11186.
31 G. G. Kresse and J. Furthmüller, Efficiency of ab-initio total energy calculations for metals and semiconductors using a plane-wave basis set, *Comput. Mater. Sci.*, 1996, **6**, 15–50.
32 J. P. Perdew, K. Burke and M. Ernzerhof, Generalized gradient approximation made simple, *Phys. Rev. Lett.*, 1996, **77**, 3865–3868.
33 J. Chadi, Special points for Brillouin-zone integrations, *Phys. Rev. B: Solid State*, 1977, **16**, 1746.
34 D. King-Smith and D. Vanderbilt, Theory of polarization of crystalline solids, *Phys. Rev. B: Condens. Matter Mater. Phys.*, 1993, **47**, 1651–1654.
35 S. Grimme, Semiempirical GGA-type density functional constructed with a long-range dispersion correction, *J. Comput. Chem.*, 2006, **27**, 1787–1799.
36 A. Togo, F. Oba and I. Tanaka, First-principles calculations of the ferroelastic transition between rutile-type and $CaCl_2$-type SiO_2 at high pressures, *Phys. Rev. B: Condens. Matter Mater. Phys.*, 2008, **78**, 134106.
37 S. Dudarev, G. Dudarev, S. Savrasov, C. Humphreys and A. Sutton, Electron-energy-loss spectra and the structural stability of nickel oxide: An LSDA + U study, *Phys. Rev. B: Condens. Matter Mater. Phys.*, 1998, **57**, 1505–1509.
38 J. Heyd, G. E. Scuseria and M. Ernzerhof, Hybrid functionals based on, a screened Coulomb potential, *J. Chem. Phys.*, 2006, **124**, 219906.
39 J. G. He and C. Franchini, Screen hybrid functional applied to $3d^0 \rightarrow 3d8$ transition-metal perovskites $LaMO_3$ (M = Sc-Cu): influence of the exchange mixing parameter on the structual, elecronic, and magnetic properties, *Phys. Rev. B: Condens. Matter Mater. Phys.*, 2012, **86**, 235117.
40 N. H. Hillebrecht, P. J. Schmidt, H. W. Rotter, G. Thiele, H. Bengel, H.-J. Cantow, S. N. Magonov and M.-H. Whangbo, Structural and scanning microscopy studies of layered compounds MCl_3 (M = Mo, Ru, Cl) and $MOCl_2$ (M = V, Nb, Mo, Ru, Os), *J. Alloys Compd.*, 1997, **246**, 70–79.
41 N. H. Miao, B. Xu, L. Zhu, J. Zhou and Z. M. Sun, 2D intrinsic ferromagnets from van der Waals antiferromagnets, *J. Am. Chem. Soc.*, 2018, **140**, 2417–2420.
42 N. D. Mermin and H. Wagner, Absence of ferromagnetism or antiferromagnetism in one- or two-dimensional isotropic Heisenberg models, *Phys. Rev. Lett.*, 1966, **17**, 1133–1136.
43 I. E. Dzyaloshinsky, A thermodynamic theory of weak ferromagnetism of antiferromagnetics, *J. Phys. Chem. Solids*, 1958, **4**, 241–255.
44 T. Moriya, Anisotropic superexchange interaction and weak ferromagnetism, *Phys. Rev.*, 1960, **120**, 91–98.
45 L. F. Lin, Q.-R. Xu, Y. Zhang, J. J. Zhang, Y. P. Liang and S. Dong, Ferroelectric ferrimagnetic $LiFe_2F_2$: Charge-ordering-mediated magnetoelectricity, *Phys. Rev. Mater.*, 2017, **1**, 071401(R).